Supplementary Information

The precise editing of surface sites on a molecular-like gold catalyst for modulating regioselectivity

Shuohao Li, Hongwei Chen, Xu Liu, Haoqi Liu, Jing Ma, and Yan Zhu

1. Experimental Section

Synthesis of gold clusters

To synthesize $Au_9(PPh_3)_8$,[S1] $NaBH_4$ (0.48 mmol) was added into $Au(PPh_3)NO_3$ (1.9 mmol) in 40 ml ethanol. The mixture was stirred at room temperature for 2 h and then filtered. Then, the dark red-brown filtrate was dissolved in CH_2Cl_2 (5 ml). Finally, the $Au_9(PPh_3)_8$ was obtained after washed with tetrahydrofuran and hexane.

To synthesize $Au_{11}(PPh_3)_8Cl_2$,[S2] 1 g $Au(PPh_3)Cl$ was added to a round-bottom flask with 55 ml of ethanol. Then, $NaBH_4$ (2.02 mmol) was added in the mixtures over 15 min. After stirring at room temperature for 2 h, the mixture was poured into hexanes and allowed to precipitate overnight. The precipitate obtained was collected and washed with hexanes and CH_2Cl_2.

To synthesize $Au_{18}(SC_6H_{11})_{14}$,[S3] $HAuCl_4 \cdot 3H_2O$ (78.8 mg) and tetraoctylammonium bromide (TOAB, 127 mg) was added to ethanol (0.5 ml) and CH_2Cl_2 (10 ml) solution. After vigorously stirring for 15 min, excess 1-cyclohexanethiol (125 ml) was added to the mixture at room temperature. Then, $NaBH_4$ (19 mg) was added drop-wise to the solution and mixture was further allowed

to react for 4-5 h under stirring. Finally, the product was washed several times with methanol to remove excess reactants. Besides, the 30 mg $Au_{18}(SC_6H_{11})_{14}$ nanoclusters and 500 mg adamantanethiolate were dissolved in 10 ml CH_2Cl_2. The solution was heated to 40 °C and maintained at this temperature with washed with CH_3OH for 3 times, vigorous stirring for 12 h. Then the solvent was removed by rotary evaporation and washed with CH_3OH for 3 times. At last, the CH_2Cl_2 was used to extract $Au_{21}(S\text{-}Adm)_{15}$ nanoclusters.

To synthesize $Au_{21}(SR)_{12}(Ph_2PCH_2PPh_2)_2$ and $Au_{23}(SR)_{16}$,[S4] $HAuCl_4 \cdot 3H_2O$ (0.3 mmol) and tetraoctylammonium bromide (0.348 mmol) were dissolved in 15 ml CH_3OH. 1-cyclohexanethiol (1.6 mmol) was added to the above mixture after 15 min. After 2 hours, $NaBH_4$ (3 mmol dissolved in 6 ml cold water) was added to the solution under vigorous stirring. After 2 days, the reaction mixture was precipitated out of CH_3OH and the $Au_{23}(SC_6H_{11})_{16}$ clusters were obtained. 20 mg $Au_{23}(SC_6H_{11})_{16}$ was dissolved in 3 ml CH_2Cl_2, and 1.2 mg $AgI(SC_6H_{11})$ was added. The reaction was allowed to proceed for 4 hours and then $Au_{23-x}Ag_x(SC_6H_{11})_{16}$ was obtained after centrifugation. Then 30 mg $Au_{23-x}Ag_x(SC_6H_{11})_{16}$ intermediate was dissolved in 6 ml CH_2Cl_2 and then 8 mg the $Au_2Cl_2(Ph_2PCH_2PPh_2)$ complex was added. The reaction was allowed to proceed for 3 hours and the $Au_{21}(SC_6H_{11})_{12}(Ph_2PCH_2PPh_2)_2$ was finally obtained.

To synthesize $Au_{24}(PPh_3)_{10}(SC_2H_4Ph)_5Cl_2$ and $Au_{25}(PPh_3)_{10}(SC_2H_4Ph)_5Cl_2$,[S5] $HAuCl_4 \cdot 3H_2O$ (0.228 mmol) and TOAB (0.265 mmol) were dissolved in 5 ml water and 10 ml toluene. After vigorously stirred for 15 min, the aqueous layer was removed

and then PPh_3 (0.686 mmol) was added under stirring. When the solution turned cloudy white, the $NaBH_4$ dissolved in ethanolic solution (0.684 mmol) was added to the whitish suspension. Then, phenylethylthiol (200 μl) was added to this solution and the reaction was allowed to proceed at 40 °C for 6 h. At the moment, the $Au_{25}(PPh_3)_{10}(SC_2H_4Ph)_5Cl_2$ clusters were obtained after washing by hexane. In order to synthesize $Au_{24}(PPh_3)_{10}(SC_2H_4Ph)_5Cl_2$, excess PPh_3 (1.2 g) was added to the product solution of $Au_{25}(PPh_3)_{10}(SC_2H_4Ph)_5Cl_2$ clusters, and then the reaction was continued for 24 h at 40 °C. The as-obtained clusters were washed with hexane and extracted with toluene, which was finally determined to be $Au_{24}(PPh_3)_{10}(SC_2H_4Ph)_5Cl_2$.

To synthesize $Au_{25}(SCH_2CH_2Ph)_{18}$,[S6] $HAuCl_4 \cdot 3H_2O$ (0.1576 g, 0.4 mmol) and TOAB (0.2558 g, 0.47 mmol) were dissolved in 15 ml tetrahydrofuran (THF). After vigorously stirring for 15 min. The mixture was cooled down to 0 ºC in an ice bath and $PhCH_2CH_2SH$ (0.17 ml, 3 equivalents of the moles of gold) was added at a very low speed over 1 h. Then, the stirring speed was changed to fast stirring, and immediately, an aqueous solution of $NaBH_4$ (0.1550 g, 4 mmol) was quickly added all at once. Finally, the $Au_{25}(SCH_2CH_2Ph)_{18}$ were obtained by washing with CH_3OH and extraction with CH_3CN. To synthesize $Au_{28}(SC_6H_{11})_{20}$, the above crude nanoclusters (10 mg) were dissolved in 0.5 ml toluene and 0.5 ml cyclohexanethiol. The reaction mixture was heated at 80 °C for 2 h and then the reaction product was washed with methanol.

To synthesize $Au_{30}(SC_4H_9)_{18}$,[S7] 100 mg of $HAuCl_4 \cdot 3H_2O$ and 87 μl of HS-tBu

were dissolved in 15 ml THF under 450 rpm for 15 min, and then an excess of 0.113 g of $NaBH_4$ in 10 ml H_2O was added. The crude product was washed with a combination of 5 ml of H_2O and 40 ml of methanol after reaction 1 h. Next, this crude product of 200 mg was combined with 1 ml of toluene and 1 ml of HS-tBu at 70 °C for 4 h. Finally, it was washed again with a combination of 5 ml of water and 40 ml of methanol.

To synthesize $Au_{38}(SC_2H_4Ph)_{24}$,[S8] firstly, $HAuCl_4 \cdot 3H_2O$ (0.5 mmol) and GSH powder (2 mmol) were mixed in 20 ml of acetone for 20 min. The mixture was cooled to 0 °C in an ice bath for 20 min. Then, a solution of $NaBH_4$ (5 mmol dissolved in 6 ml of cold water) was rapidly added. Finally, the black $Au_n(SG)_m$ nanoclusters were found to precipitate out. A solution of 200 mg $Au_n(SG)_m$ (dissolved in 6 ml of water) was mixed with ethanol (0.3 ml), toluene (2 ml) and phenylethylthiol (2 ml) and then maintained at 80 °C under air atmosphere for 10 min. Finally, the thermal process was allowed to continue for 40 h at 80 °C and $Au_{38}(SC_2H_4Ph)_{24}$ clusters was obtained after washed with ethanol.

To synthesize $Au_{36}(SPh\text{-}Bu^t)_{24}$,[S9] 10 mg $Au_{38}(SC_2H_4Ph)_{24}$ were dissolved in 0.5 mL toluene and 0.5 ml HSPh-4-Bu^t. Then, the mixture was heat to 80 °C for 12 h. After that, the crude product was treated in the same method as for $Au_{38}(SC_2H_4Ph)_{24}$ to obtain $Au_{36}(SPh\text{-}Bu^t)_{24}$.

To synthesize $Au_{44}(SPh\text{-}Bu^t)_{28}$,[S10] $HAuCl_4$ (0.125 mmol) and 4-tertbutylbenzenethiol (0.625 mmol) were dissolved in 10 ml of THF. When the solution was cooled in an ice bath, the fresh $NaBH_4$ (1.25 mmol dissolved in 1 ml of

H_2O) was rapidly added. After 24 h, the $Au_x(SPh\text{-}Bu^t)_y$ intermediates were washed with methanol and extracted with CH_2Cl_2. Then the $Au_x(SPh\text{-}Bu^t)_y$ intermediates were dissolved in 0.5 ml of toluene and 0.1 ml 4-tertbutylbenzenethiol and size-focused at 60 °C for 24 h. Finally, the $Au_{44}(SPh\text{-}Bu^t)_{28}$ clusters were separated from the reaction mixture by methanol and extracted with CH_2Cl_2.

To synthesize $Au_{144}(SCH_2Ph)_{60}$,[S11] $HAuCl_4 \cdot 4H_2O$ (0.607 mmol) and TOAB (0.696 mmol) were added to the 30 ml of MeOH. After being vigorously stirred for 30 min, $PhCH_2SH$ (3.19 mmol) were added to the solution at room temperature. After ~15 min, a fresh $NaBH_4$ solution (6 mmol dissolved in 10 ml of nanopure water) was rapidly added to the solution under vigorous stirring. The reaction was stopped after ~4.5 h, and then the solution was removed. Black precipitates were washed with excess methanol and collected by centrifugation.

To synthesis of the $Au_{22}(dppo)_6$ (dppo = 1,8-bis(diphenylphosphino)octane),[S12] a solution of dppo (0.104 g) in acetone was added to a suspension of $[AuCl(SMe)_2]$ (0.127 g) in acetone. The mixture was stirred for 2 h before rotary evaporator, which was collected by filtration, with diethyl ether and dried under vacuum. Then, a dichloromethane solution (180 ml) of $Au_2dppoCl_2$ (142 mg) was cooled to 0 °C in an ice bath over a period of 30 min under magnetic stirring, and an ethanol solution (8 ml) of $NaBH_4$ (22.7 mg) was quickly added. The mixture was stirred at 0 °C for 24 h. After removal of the solvent, the dark brown residue denoted as $Au_{22}(dppo)_6$ was washed by a dichloromethane and hexane mixed solution. The $Au_{22}(dppo)_6$ was crystallized by ethyl ether diffusion into a dichloromethane/methanol (5:1) solution.

Catalytic test

Gold clusters (2 mg) were added to a mixture of triethylamine (1.28 mmol) and phenylacetylene (0.15 mmol) in a round-bottomed flask containing 2 ml acetonitrile solvent. After stirring for 30 min at room temperature, benzyl azide (0.15 mmol) was added into the above mixture. Subsequently, the reaction mixture was placed over an oil bath at 80 °C for 5 h. The reaction solvent was evaporated to obtain the crude product. The regioselectivity of the crude product was calculated by ^{1}H NMR spectroscopic analysis. Besides, the same reactions were performed with various organic alkynes that contained electron-donating and -withdrawing groups.

TON is calculated according to the following formula:

$$\mathrm{TON} = \frac{Conversion \times n_{\mathrm{substrate}}}{\frac{m_{cluster}}{M_{cluster}}}$$

$n_{substrate}$ = the moles of substrate (mol);

$m_{cluster}$ = the amount of cluster (mg);

$M_{cluster}$ = the formula weight of cluster (mg/mol).

Characterization

The UV-vis absorption spectra were carried out on a UV-1800 spectrophotometer (Shimadzu, Japan). ESI mass spectra were recorded on a Waters QT of mass spectrometer using a Z-spray source. The sample was first dissolved in toluene (~0.5 mg/ml) and directly infused into the chamber at 5 μl/min. The source temperature was kept at 70 °C, the spray voltage was 2.20 kV, and the cone voltage was adjusted to 60 V. The binding energies of the surface species on the catalysts were determined by X-ray photoelectron spectroscopy (XPS) (Thermo Scientific K-Alpha)

using Al Kα (hυ = 1486.6 eV) as the excitation source. Correction of the charge effect was made with the C (1s) peak at 284.8 eV. The X-ray absorption fine structure (XAFS) spectra at Au K-edge were measured at BL14W1 beamline of Shanghai Synchrotron Radiation Facility (SSRF). They were operated at 3.5 GeV under "top-up" mode with a constant current of 260 mA. The energy was calibrated accordingly to the absorption edge of pure Au foil. Athena and Artemis codes were used to analyze the data and fit the profiles. FT-IR spectra of CO adsorbed were recorded using an FT-IR NICOLET iS10 (Thermo Fisher Scientific Inc.) provided with a cell (Praying Mantis, Harrick) and liquid nitrogen cooled MCT detector. The catalysts were loaded into the cell and then purged under Ar flow for 1 hour at 150 ^{o}C. After the catalysts were cooled to analysis temperature, a background spectrum was first collected in Ar atmosphere and then exposed CO (99.999%) at 298 K for 30 min. After saturation adsorption, the data were collected under Ar flow with 20 ml/min. The ^{1}H NMR spectra were recorded on a Bruker ARX-400 spectrometer. Chemical shifts were reported in ppm relative to the internal solvent peak (δ = 7.26 ppm, for $CDCl_3$). The reaction products were dissolved into $CDCl_3$ and analyzed by ^{1}H NMR.

2. Computational Details

All the molecular model calculations were carried out by using the Gaussian 09 program (Revision E.01)[S13] with the B3LYP functional. The surface area analysis was employed using the Multiwfn soft package.[S14] We adopted two kinds of models, i.e., model A: simplified models of Au_{21} (S-Au_{21}) and Au_{23} (S-Au_{23}); model B: all-atom models of Au_{21} (A-Au_{21}) and Au_{23} (A-Au_{23}) in our computations.

3. Supporting Figures and Tables

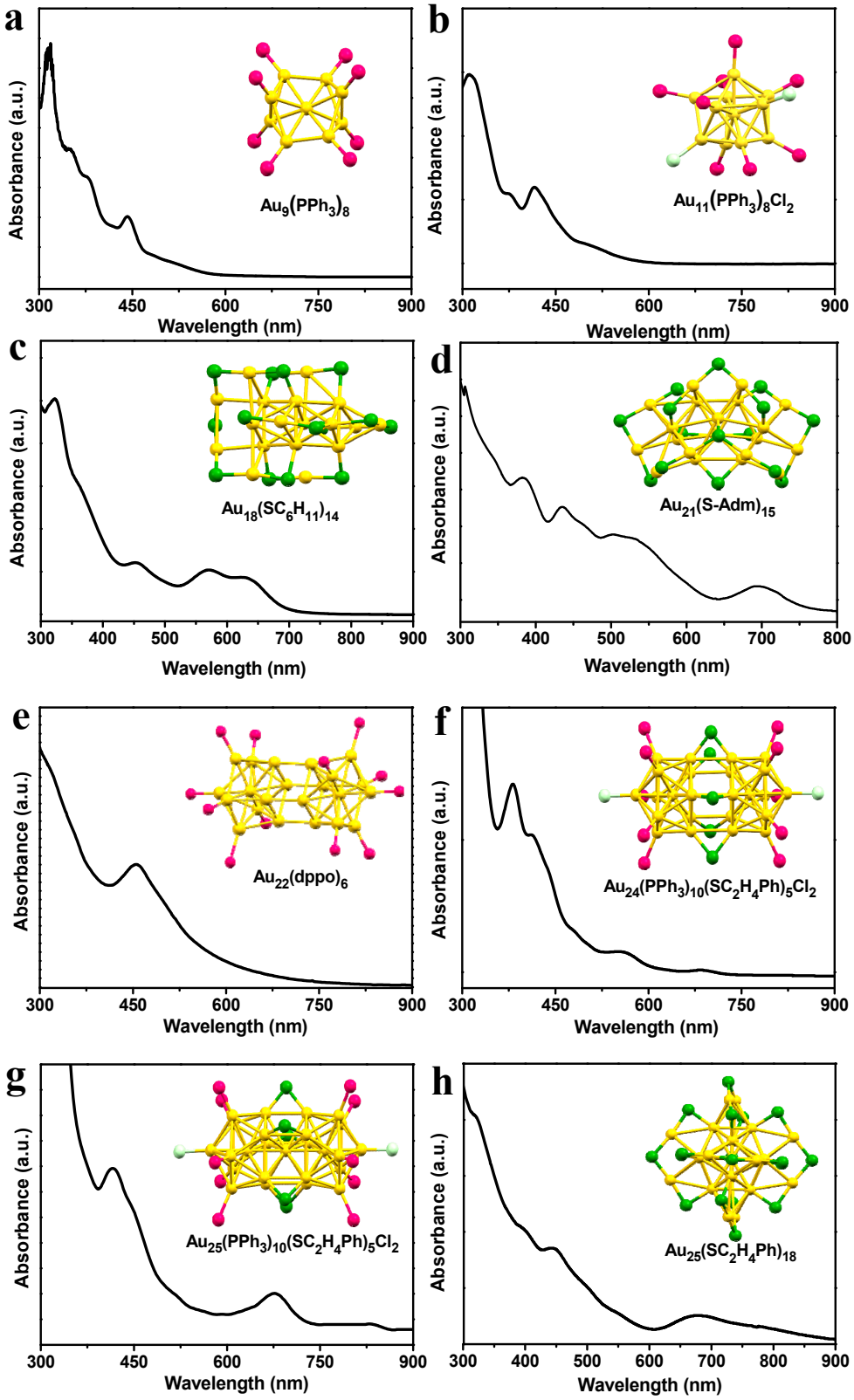

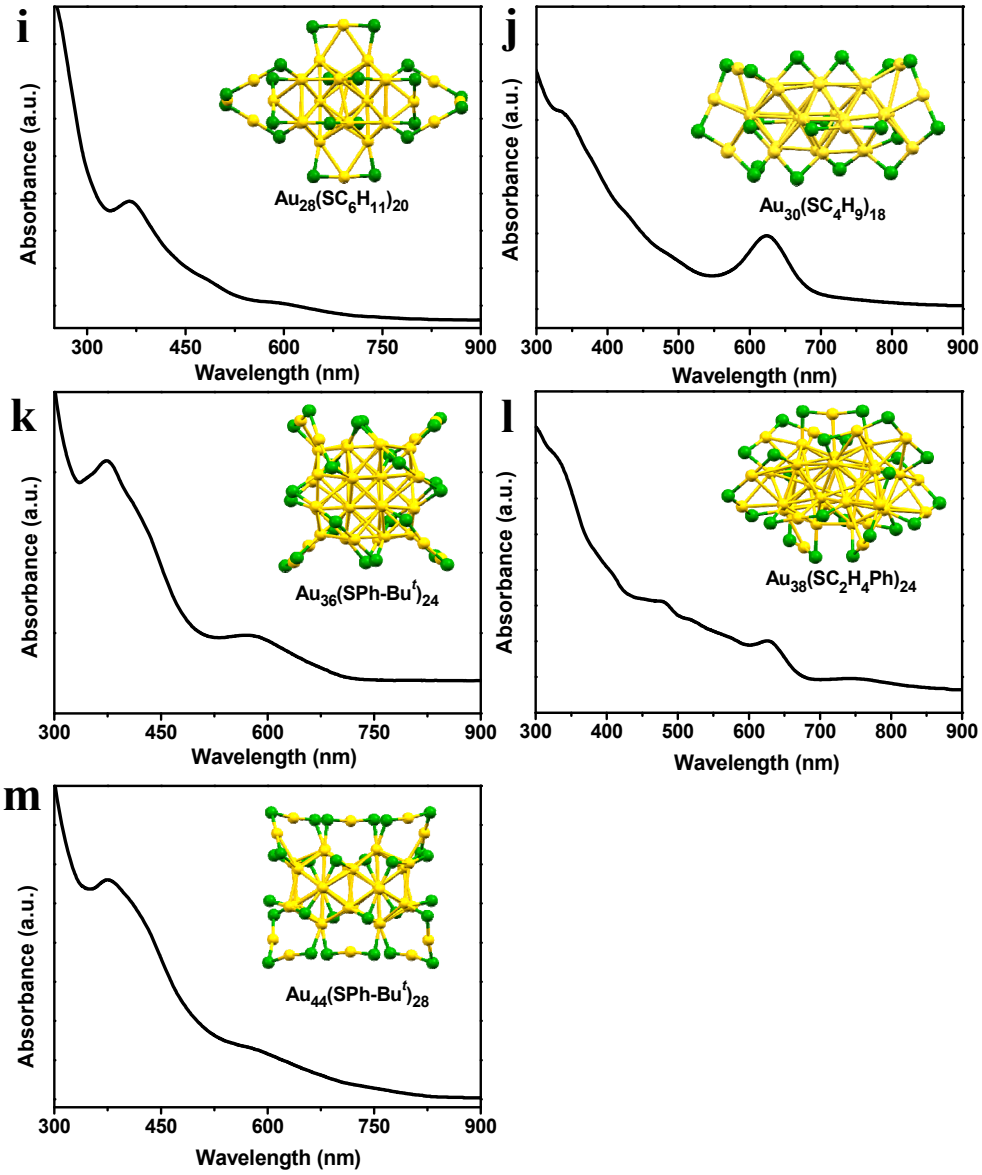

Fig. S1 UV-vis spectra of (a) $Au_9(PPh_3)_8$, (b) $Au_{11}(PPh_3)_8Cl_2$, (c) $Au_{18}(SC_6H_{11})_{14}$, (d) $Au_{21}(S\text{-}Adm)_{15}$, (e) $Au_{22}(dppo)_6$, (f) $Au_{24}(PPh_3)_{10}(SC_2H_4Ph)_5Cl_2$, (g) $Au_{25}(PPh_3)_{10}(SC_2H_4Ph)_5Cl_2$, (h) $Au_{25}(SC_2H_4Ph)_{18}$, (i) $Au_{28}(SC_6H_{11})_{20}$, (j) $Au_{30}(SC_4H_9)_{18}$, (k) $Au_{36}(SPh\text{-}Bu^t)_{24}$, (l) $Au_{38}(SC_2H_4Ph)_{24}$, and (m) $Au_{44}(SPh\text{-}Bu^t)_{28}$. Color codes: yellow = Au; green = S; pink = P; light green = Cl. Insets are corresponding atomic structures of gold clusters.

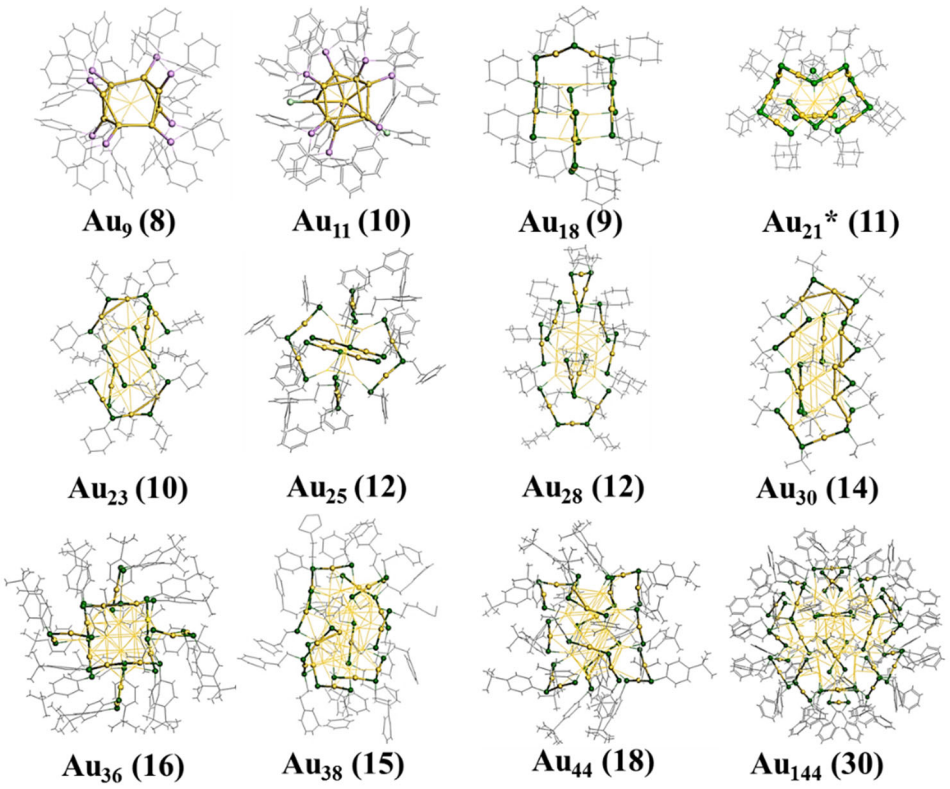

Fig. S2 The details of surface Au atoms in ligand-protected Au_n clusters with different atomic structures and surface motifs. The numbers in brackets denote the surface Au atom numbers. Color codes: yellow = Au; green = S; pink = P; light green = Cl.

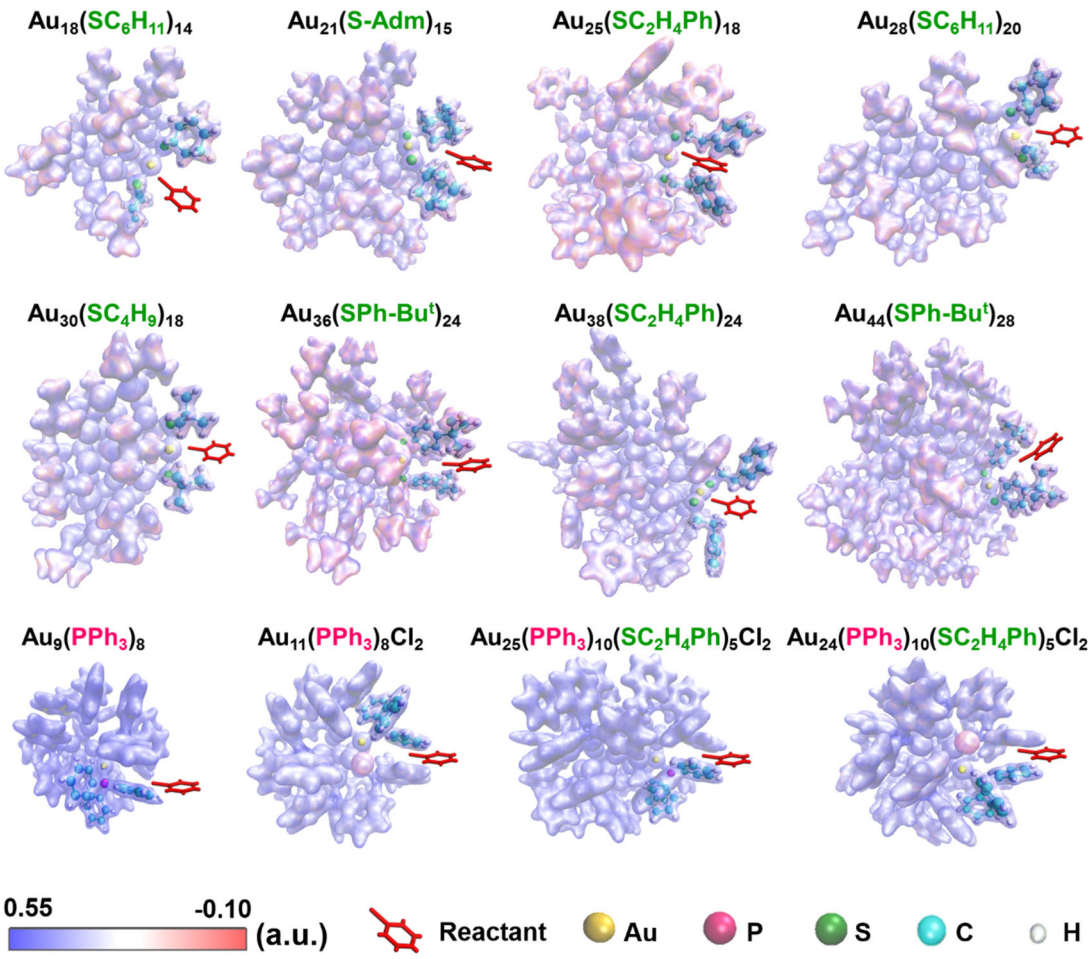

Fig. S3 The electrostatic potentials of the Au_n clusters and the steric hindrance from thiolate/PPh_3 ligands.

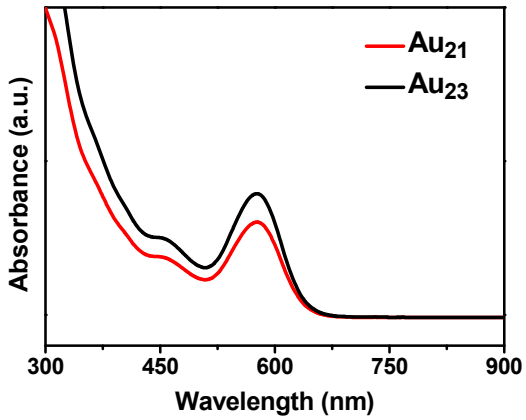

Fig. S4 UV-vis spectra of $Au_{23}(SC_6H_{11})_{16}$ and $Au_{21}(SC_6H_{11})_{12}(Ph_2PCH_2PPh_2)_2$.

Table S1. The calculated surface area/ligand in the Au_n clusters[a]

Samples	Surface area ($Å^2$)	Number of ligands (N)	Surface area/ligand ($Å^2$/N)
$Au_9(PPh_3)_8$	1468.00	8	183.50
$Au_{11}(PPh_3)_8Cl_2$	1455.71	10	145.57
$Au_{18}(SC_6H_{11})_{14}$	1423.17	14	101.66
Au_{21}(S-Adm)$_{15}$	1867.43	15	124.50
$Au_{21}(SC_6H_{11})_{12}(Ph_2PCH_2PPh_2)_2$	1779.18	14	127.08
$Au_{23}(SC_6H_{11})_{16}$	1674.99	16	104.69
$Au_{24}(PPh_3)_{10}(SC_2H_4Ph)_5Cl_2$	1997.58	17	117.50
$Au_{25}(PPh_3)_{10}(SC_2H_4Ph)_5Cl_2$	2054.12	17	120.83
$Au_{25}(SC_2H_4Ph)_{18}$	1983.74	18	110.21
$Au_{28}(SC_6H_{11})_{20}$	1925.08	20	96.25
$Au_{30}(SC_4H_9)_{18}$	1444.83	18	80.27
Au_{36}(SPh-Bu^t)$_{24}$	2963.17	24	123.47
$Au_{38}(SC_2H_4Ph)_{24}$	2523.00	24	105.13
Au_{44}(SPh-Bu^t)$_{28}$	3370.21	28	120.36

[a]The surface area analysis was employed using the Multiwfn soft package.[S14]

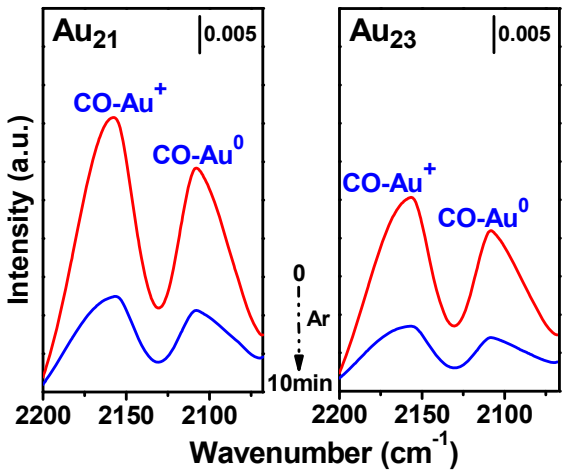

Fig. S5 Time-resolved in situ FT-IR spectra of CO adsorbed onto $Au_{21}(SC_6H_{11})_{12}(Ph_2PCH_2PPh_2)_2$ and $Au_{23}(SC_6H_{11})_{16}$.

The chemical adsorption capabilities of the $Au_{21}(SC_6H_{11})_{12}(Ph_2PCH_2PPh_2)_2$ and $Au_{23}(SC_6H_{11})_{16}$ clusters were detected by in situ FT-IR spectroscopy of CO adsorbed onto the two catalysts. As shown in Fig. S5, CO molecules adsorbed onto the gold clusters exhibited two primary bands at 2107 and 2157 cm^{-1}: the former is assigned to CO adsorbed on metallic Au sites;[S15] the latter is attributed to CO adsorbed on the positive Au^+ sites.[S16,S17] Especially, the intensity of the chemical adsorption of CO over $Au_{21}(SC_6H_{11})_{12}(Ph_2PCH_2PPh_2)_2$ was higher than that over $Au_{23}(SC_6H_{11})_{16}$, which clarified that the $Au_{21}(SC_6H_{11})_{12}(Ph_2PCH_2PPh_2)_2$ cluster had higher surface adsorption capability, exhibiting more effective activity.[S18]

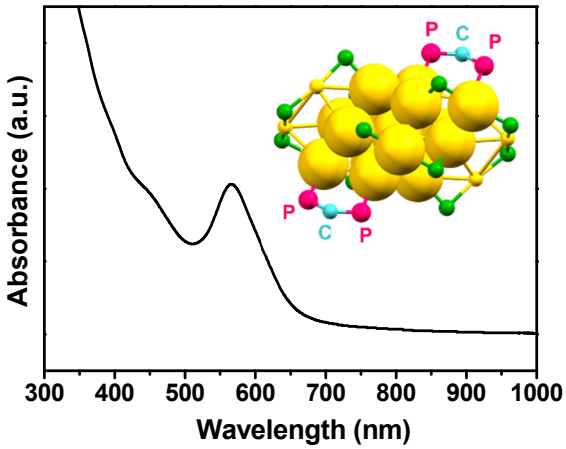

Fig. S6 UV-vis spectrum of the $Au_{21}(SC_6H_{11})_{12}(Ph_2PCH_2PPh_2)_2$ cluster after reaction.

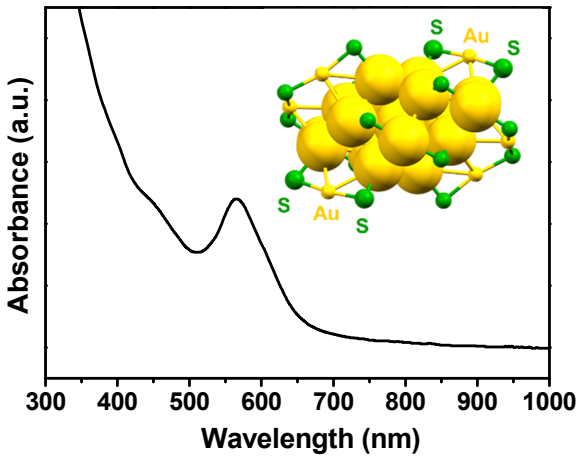

Fig. S7 UV-vis spectrum of the $Au_{23}(SC_6H_{11})_{16}$ cluster after reactions.

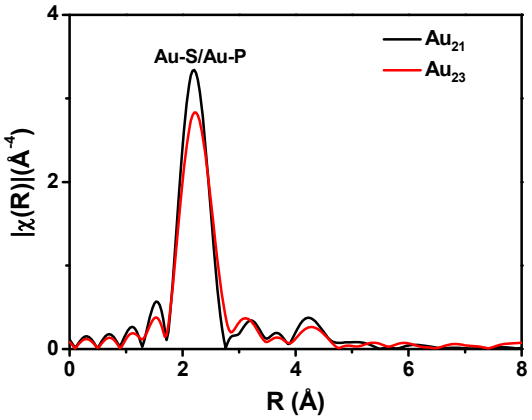

Fig. S8 EXAFS profiles of $Au_{21}(SC_6H_{11})_{12}(Ph_2PCH_2PPh_2)_2$ and $Au_{23}(SC_6H_{11})_{16}$.

The changes in the gold charge state were also monitored by X-ray absorption near edges structure (XANES) studies (Fig. 5b). The white line intensities of $Au_{21}(SC_6H_{11})_{12}(Ph_2PCH_2PPh_2)_2$ and $Au_{23}(SC_6H_{11})_{16}$ are higher than Au foil obviously, which was generally caused by the interactions ligands and gold occurred on the surface of Au clusters.[S19,S20] The Au L_3-edge white line derives from electronic transition from occupied 2p to unoccupied 5d states, where a less intense white line corresponds to higher 5d electronic density.[S21] Therefore, the $Au_{21}(SC_6H_{11})_{12}(Ph_2PCH_2PPh_2)_2$ and $Au_{23}(SC_6H_{11})_{16}$ have similar 5d electronic density because of consistency of white line intensities between them. Furthermore, local coordination environments in $Au_{21}(SC_6H_{11})_{12}(Ph_2PCH_2PPh_2)_2$ and $Au_{23}(SC_6H_{11})_{16}$ were probed by extended X-ray absorption fine structure (EXAFS) experiments. As shown in Fig. S8, Au-S and Au-P bonds can be observed but the Au-Au bonds in either Au_{21} or Au_{23} disappeared in EXAFS spectra, probably due to the thermal fluctuation of Au–Au bonds at room temperature.[S22]

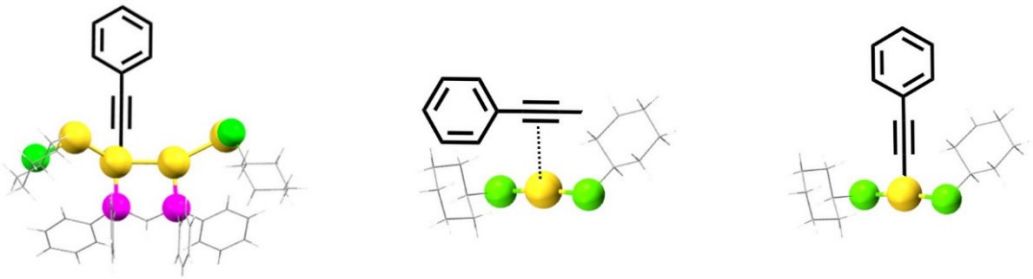

Fig. S9 Binding modes of alkyne on the gold clusters.

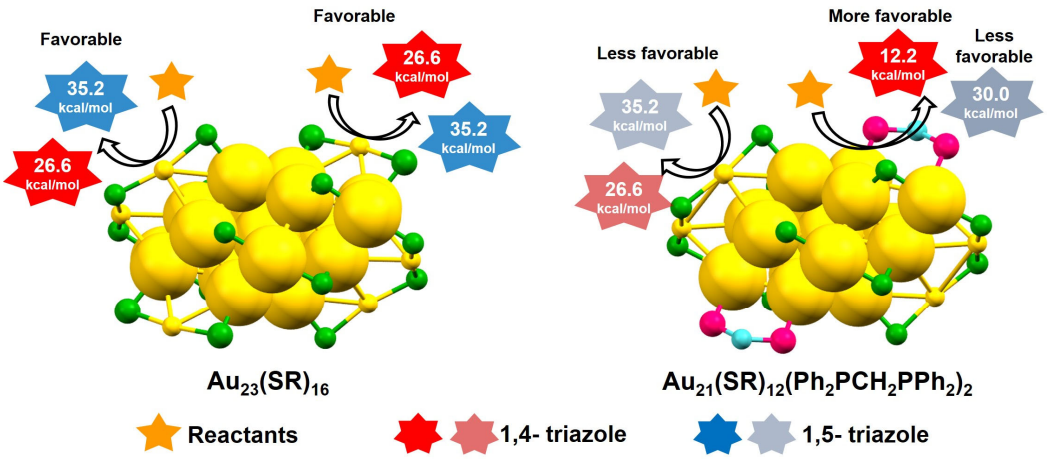

Fig. S10 The diagram for the click reaction of alkynes and benzyl azide on the surface sites of the $Au_{23}(SC_6H_{11})_{16}$ and $Au_{21}(SC_6H_{11})_{12}(Ph_2PCH_2PPh_2)_2$ clusters. Color codes: yellow = Au; green =S; pink = P; blue = C.

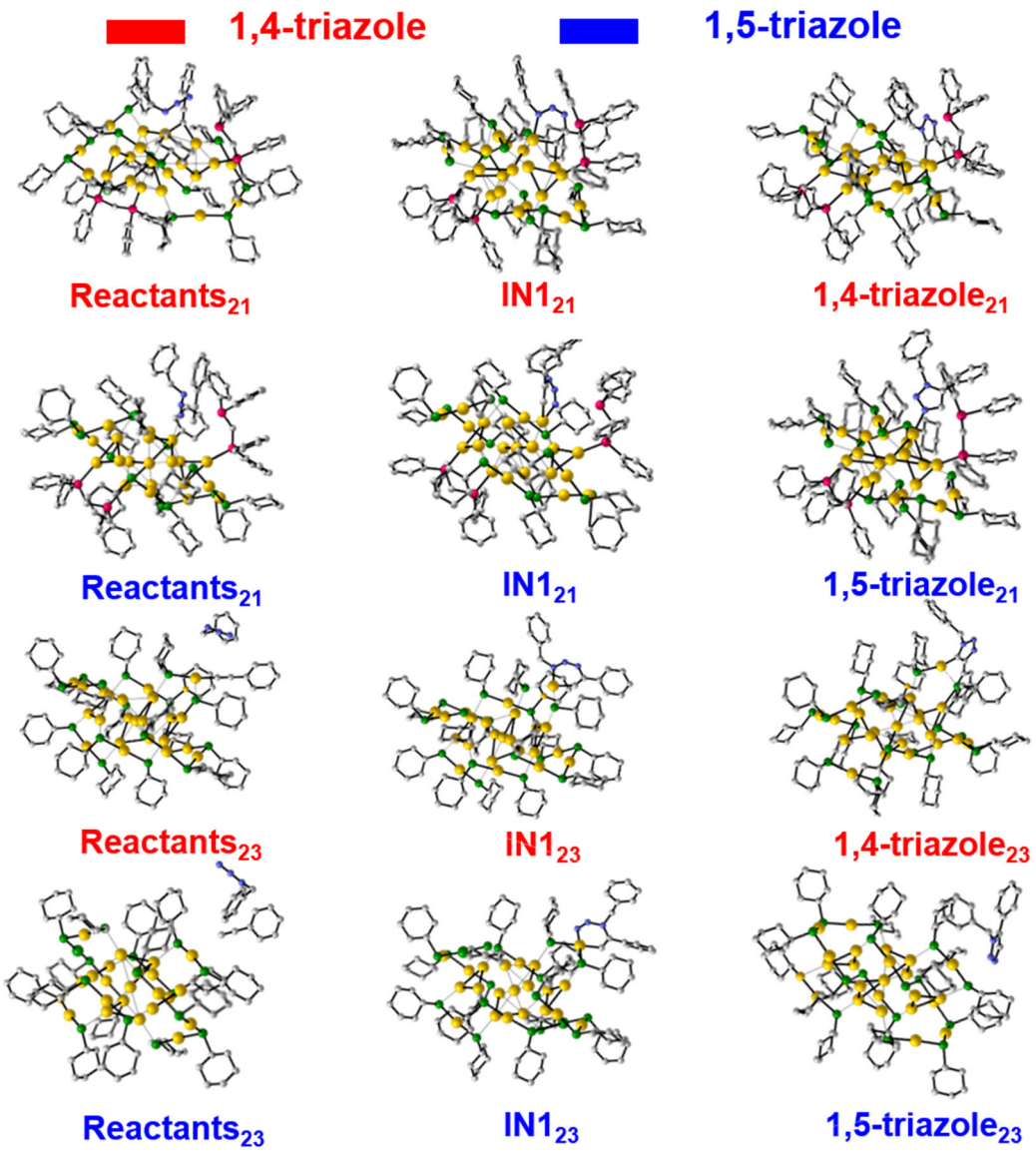

Fig. S11 Optimized structures of the A-Au21 and A-Au23 models involved in the reaction of the reactants and the formation of the intermediates and products. Color codes: yellow = Au, green = S, pink = P, gray = C, blue = N. To make the structural models relatively sharper, all the hydrogen atoms were hidden.

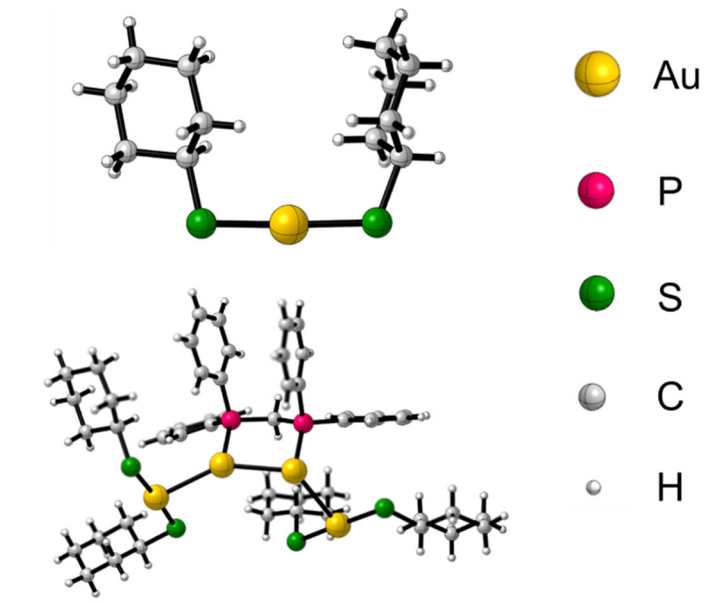

Fig. S12 The simplified model structures of Au_{23} (top) and Au_{21} (bottom).

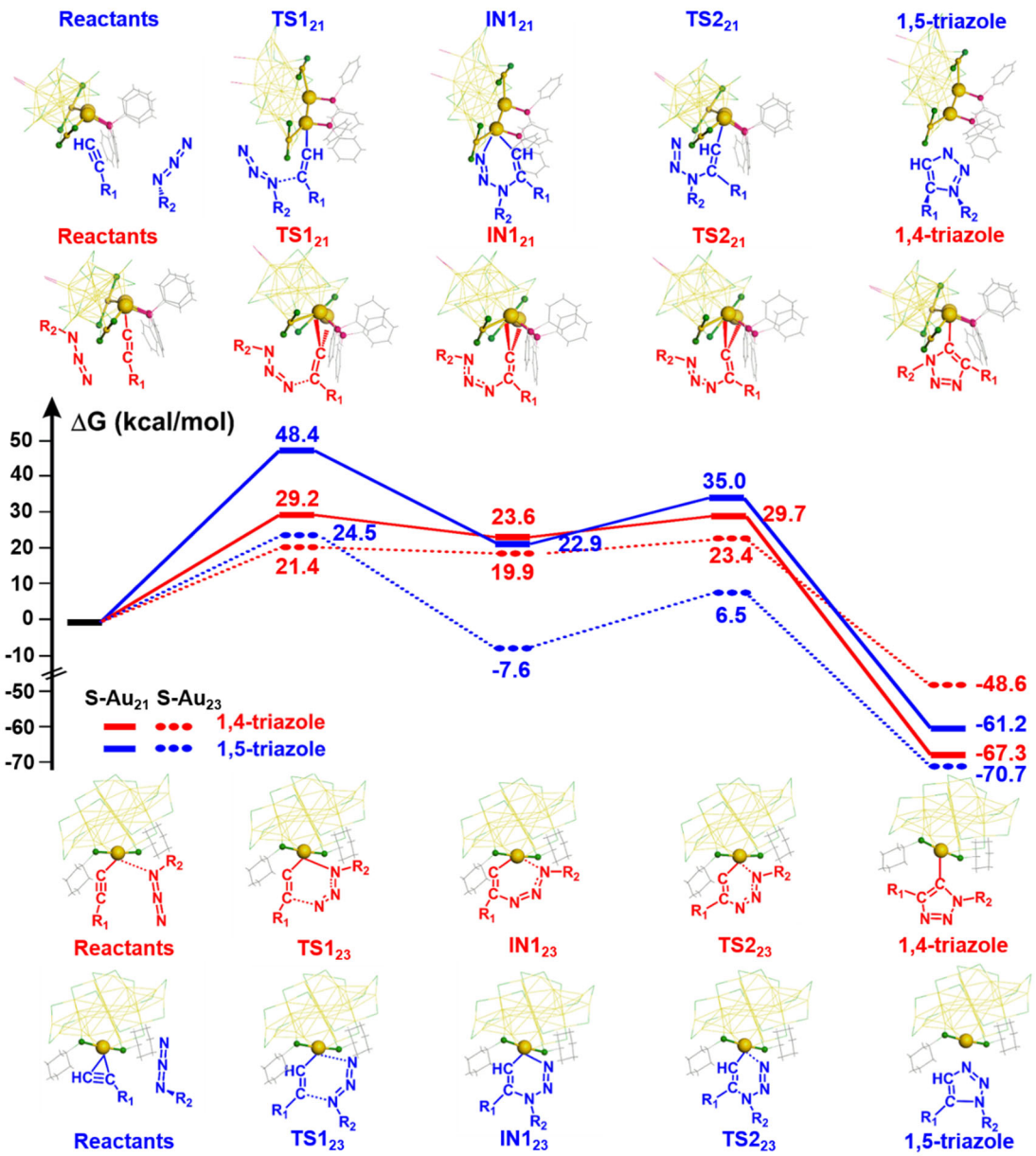

Fig. S13 The calculated energy profiles for the potential reaction pathways of phenylacetylene and benzyl azide on the simplified S-Au$_{23}$ and S-Au$_{21}$ models. Color codes: yellow = Au; green = S; pink = P. TS = transition state; IN = intermediate.

During the geometry optimizations of the medium-sized systems like S-Au$_{21}$ and S-Au$_{23}$, the 6-31G(d) basis set was selected for S, P, C, H atoms and LANL2DZ basis set was selected for Au element. Moreover, in the DFT calculations of large-sized all-atom models of A-Au$_{21}$ and A-Au$_{23}$, the 6-31G basis set was selected for S, P, C, H

atoms. It is acceptable that the hydrogen atom on the phenylacetylene is deprotonated for the 1,4-triazole.[S23] Besides, the calculated harmonic vibrational frequencies were scaled to 0.96.[S24] The transition state was identified to have only one imaginary frequency value in the vibrational frequency calculations.

In the first step, we adopted the simplified model A to search the possible reaction pathways. The structures Au-S-Au and Au-Au$_P$-P-P-Au$_P$-Au (Au$_P$ denotes the Au atom attached to the phosphine ligand) were assumed to be the possible active sites for the attacking of reactants. Thus, the simplified S-Au$_{23}$ and S-Au$_{21}$ models were built to contain the reaction sites, neglecting the effects of the other inert Au atoms and ligands, as shown in Fig. S12. For the simplified models S-Au$_{23}$, all the atoms were allowed to relax during the geometry optimization, and their possible reaction paths were presented in Fig. S13 (the free energies of each simplified models were listed in the Table S2 and S3). However, Au$_{21}$ has larger conformation flexibility than Au$_{23}$. Thus, in the simplified model S-Au$_{21}$, the distance of Au$_P$-Au$_P$ was fixed to prevent the dissociation of Au-Au interaction, while all the other atoms are free throughout the whole optimization process.

Finally, we used the all-atom models A-Au$_{21}$ and A-Au$_{23}$ in DFT calculations (the free energies of each all-atom models were listed in the Table S4 and S5). It was found that the distance of Au$_P$-Au$_P$ occurred a great change, so that one of the Au$_P$ was away from the phosphine ligands, and the catalytic reaction of phenylacetylene and benzyl azide occurs on this gold atom. Compared with the simplified model S-Au$_{23}$, the structure of intermediate products in A-Au$_{23}$ is similar to that of S-Au$_{23}$.

The energy profile for the reaction of A-Au_{23} were illustrated in Fig. 6. The energy difference $\Delta\Delta G$ = 8.6 kcal/mol between the reaction pathway toward 1,4-product and that toward 1,5-product was colsed to that in S-Au_{23} model ($\Delta\Delta G$ = 3.1 kcal/mol).

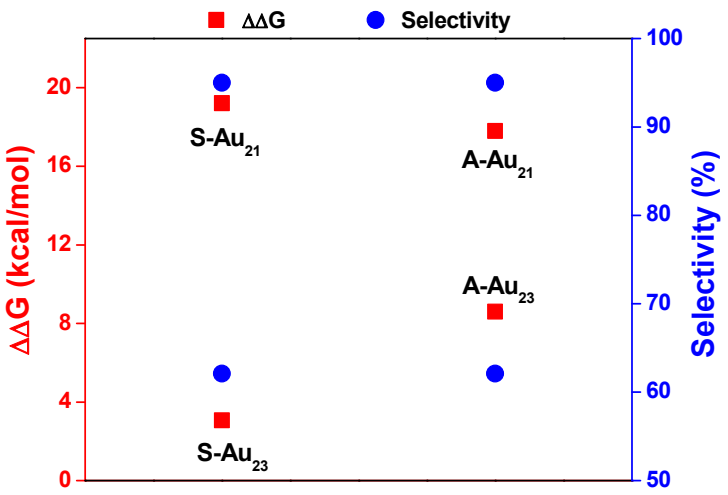

Fig. S14 Correlation between ΔΔG ($\Delta G(TS1_{1,4\text{-triazole}}) - \Delta G(TS1_{1,5\text{-triazole}})$) and the 1,4-triazole selectivity over the two modeled Au_{21} and Au_{23}.

Table S2 The free energies of S-Au_{21} in this work

Models	Free energies (Hartree)
S-Au_{21}-1,4-reactant	-5466.325516
S-Au_{21}-1,4-TS1	-5466.278978
S-Au_{21}-1,4-IN1	-5466.278978
S-Au_{21}-1,4-TS2	-5466.27823
S-Au_{21}-1,4-triazole	-5466.395033
S-Au_{21}-1,5-reactant	-5466.964689
S-Au_{21}-1,5-TS1	-5466.887552
S-Au_{21}-1,5-IN1	-5466.928186
S-Au_{21}-1,5-TS2	-5466.908941
S-Au_{21}-1,5-triazole	-5467.062186

Table S3 The free energies of S-Au_{23} in this work

Models	Free energies (Hartree)
S-Au_{23}-1,4-reactant	-2144.843621
S-Au_{23}-1,4-TS1	-2144.809512
S-Au_{23}-1,4-IN1	-2144.809512
S-Au_{23}-1,4-TS2	-2144.806335
S-Au_{23}-1,4-triazole	-2144.921045
S-Au_{23}-1,5-reactant	-2145.447946
S-Au_{23}-1,5-TS1	-2145.408955
S-Au_{23}-1,5-IN1	-2145.460035
S-Au_{23}-1,5-TS2	-2145.437633
S-Au_{23}-1,5-triazole	-2145.56068

Table S4 The free energies of A-Au_{21} in this work

Models	Free energies (Hartree)
A-Au_{21}-1,4-reactant	-14483.265711
A-Au_{21}-1,4-TS1	-14483.246238
A-Au_{21}-1,4-IN1	-14483.253945
A-Au_{21}-1,4-TS2	-14483.248936
A-Au_{21}-1,4-triazole	-14483.253945
A-Au_{21}-1,5-reactant	-14483.918905
A-Au_{21}-1,5-TS1	-14483.871032
A-Au_{21}-1,5-IN1	-14483.904198
A-Au_{21}-1,5-TS2	-14483.899178
A-Au_{21}-1,5-triazole	-14484.008410

Table S5 The free energies of A-Au_{23} in this work

Models	Free energies (Hartree)
A-Au_{23}-1,4-reactant	-13991.670362
A-Au_{23}-1,4-TS1	-13991.627925
A-Au_{23}-1,4-IN1	-13991.631951
A-Au_{23}-1,4-TS2	-13991.625864
A-Au_{23}-1,4-triazole	-13991.744907
A-Au_{23}-1,5-reactant	-13992.295139
A-Au_{23}-1,5-TS1	-13992.239095
A-Au_{23}-1,5-IN1	-13992.290774
A-Au_{23}-1,5-TS2	-13992.269809
A-Au_{23}-1,5-triazole	-13992.385695

4. Supporting References

S1 F. Wen, U. Englert, B. Gutrath and S. Ulrich, *Eur. J. Inorg. Chem*., 2008, **2008**, 106-111.

S2 L. McKenzie, T. Zaikova and J. Hutchison, *J. Am. Chem. Soc*., 2014, **136**, 13426-13435.

S3 S. Chen, L. Xiong, S. Wang, Z. Ma, S. Jin, H. Sheng, Y. Pei and M. Zhu, *J. Am. Chem. Soc.*, 2016, **138**, 10754-10757.

S4 A. Das, T. Li, K. Nobusada, C. Zeng, N. L. Rosi and R. Jin, *J. Am. Chem. Soc*., 2013, **135**, 18264-18267.

S5 A. Das, T. Li, K. Nobusada, Q. Zeng, N. Rosi and R. Jin, *J. Am. Chem. Soc*., 2012, **134**, 20286-20289.

S6 Y. Chen, C. Liu, Q. Tang, C. Zeng, T. Higaki, A. Das, D. Jiang, N. Rosi and R. Jin, *J. Am. Chem. Soc.*, 2016, **138**, 1482-1485.

S7 D. Crasto and A. Dass, *J. Phys. Chem. C*., 2013, **117**, 22094-22097.

S8 H. Qian, Y. Zhu and R. Jin, *ACS Nano*, 2009, **3**, 3795-3803.

S9 C. Zeng, H. Qian, T. Li, G. Li, N. Rosi, B.Yoon, R. Barnett, R. Whetten, U. Landman and R. Jin, *Angew. Chem. Int. Ed*., 2012, **51**, 13114-13118.

S10 C. Zeng, Y. Chen, K. Iida, K. Nobusada, K. Kirschbaum, K. Lambright and R. Jin, *J. Am. Chem. Soc.*, 2016, **138**, 3950-3953.

S11 N. Yan, N. Xia, L. Liao, M. Zhu, F. Jin, R. Jin and Z. Wu, *Sci. Adv.*, 2018, **4**, e7259.

S12 J. Chen, Q. Zhang, T. A. Bonaccorso, P. G. Williard and L. Wang, *J. Am. Chem. Soc.*, 2014, **136**, 92-95.

S13 M. J. Frisch, G. W. Trucks, H. B. Schlegel, G. E. Scuseria, M. A. Robb, J. R. Cheeseman, G. Scalmani, V. Barone, B. Mennucci, G. A. Petersson, H. Nakatsuji, M. Caricato, X. Li, H. P. Hratchian, A. F. Izmaylov, J. Bloino, M. Sonnenberg, M. Hada, K. Ehara, R. Toyota, J. Fukuda, M. Hasegawa, T. Ishida, Y. Nakajima, O. Honda, H. Kitao, T. Nakai, J. Vreven, A. J. Montgomery, J. E. Peralta, F. Ogliaro, M. Bearpark, J. J. Heyd, E. Brothers, K. N. Kudin, V. N. Staroverov, T. Keith, R. Kobayashi, J. Normand, K. Raghavachari, A. Rendell, J. C. Burant, S. S. Iyengar, J. Tomasi, M. Cossi, N. Rega, J. M. Millam, M. Klene, J. E. J. Knox, B. Cross, V. Bakken, C. Adamo, J. Jaramillo, R. Gomperts, R. E.

Stratmann, O. Yazyev, A. J. Austin, R. Cammi, C. Pomelli, J. W. Ochterski, R. L. Martin, K. Morokuma, V. G. Zakrzewski, G. A. Voth, P. Salvador, J. J. Dannenberg, S. Dapprich, A. D. Daniels, O. Farkas, J. B. Foresman, J. V. Ortiz, J. Cioslowski and D. J. Fox, Gaussian, Inc., Wallingford CT, 2013.

S14 T. Lu and F. Chen, *J. Comput. Chem.*, 2012, **33**, 580-592.

S15 H. Masatake and M. Daté, *Appl. Catal. A: Gen*., 2001, **222**, 427-437.

S16 Z. Wu, S. Zhou, H. Zhu, S. Dai and S. Overbury, *J. Phys. Chem. C*, 2009, **113**, 3726-3734.

S17 Z. Wu, D. Jiang, A. Mann, D. Mullins, Z. Qiao, L. Allard, C. Zeng, R. Jin and S. Overbury, *J. Am. Chem. Soc*., 2014, **136**, 6111-6122.

S18 X. Ren, M. Guo, H. Li, C. Li, L.Yu, J. Liu and Q. Yang, *Angew. Chem. Int. Ed.*, 2019, **58**, 14483-14488.

S19 D. M. Chevrier, A. Chatt, P. Zhang, C. Zeng and R. Jin, *J. Phys. Chem. Lett.*, 2013, **4**, 3186-3191.

S20 D. M. Chevrier, C. Zeng, R. Jin, A. Chatt and P. Zhang, *J. Phys. Chem. C*, 2015, **119**, 1217-1223.

S21 G. A. Simms, J. D. Padmos and P. Zhang, *J. Chem. Phys.*, 2009, **131**, 214703.

S22 P. Zhang, *J. Phys. Chem. C*., 2014, **118**, 25291-25299.

S23 S. Rej, K. Chanda, C. Chiu and M. Huang, *Chem. Eur. J*., 2014, **20**, 15991-15997.

S24 R. D. Johnson III and E. Nist, NIST standard reference database, 2019.